Mechanical Defects Detection on Solar Panel with Ultrasonic Guided Waves

Dicky Silitonga, Nico Declercq, Pascal Pomarède, Fodil Meraghni

▶ **To cite this version:**

Dicky Silitonga, Nico Declercq, Pascal Pomarède, Fodil Meraghni. Mechanical Defects Detection on Solar Panel with Ultrasonic Guided Waves. 16ème Congrès Français d'Acoustique, CFA2022, Société Française d'Acoustique; Laboratoire de Mécanique et d'Acoustique, Apr 2022, Marseille, France. hal-03847754

HAL Id: hal-03847754
https://hal.science/hal-03847754

Submitted on 10 Nov 2022

HAL is a multi-disciplinary open access archive for the deposit and dissemination of scientific research documents, whether they are published or not. The documents may come from teaching and research institutions in France or abroad, or from public or private research centers.

L'archive ouverte pluridisciplinaire **HAL**, est destinée au dépôt et à la diffusion de documents scientifiques de niveau recherche, publiés ou non, émanant des établissements d'enseignement et de recherche français ou étrangers, des laboratoires publics ou privés.

16ème Congrès Français d'Acoustique
11-15 Avril 2022, Marseille

Crack detection on solar photovoltaic module with ultrasonic guided waves

D. Silitonga [a], N. Declercq [a], P. Pomarède [a] F. Meraghni [b]
[a] Georgia Tech-Lorraine - CNRS IRL 2958, Metz
[b] Ecole Nationale Supérieure d'Arts et Métiers (ENSAM), Metz

In order to ensure a solar power system runs at its optimum efficiency throughout the lifecycle, proper structural health monitoring on photovoltaic module (PVM) should be performed as part predictive maintenance activities. Mechanical defects such as cracks may induce power loss, raise the risks of electrical failure, and compromise the PVM's structural integrity. Therefore, early detection of their existence is crucial. This research emphasizes the utilization of ultrasonic guided waves (UGW) to develop an efficient inspection technique. Since the waves can travel over large distances, they allow long-range defect detection, hence faster inspection process as compared to the conventional bulk wave scan. In this work, UGW experiments were done over areas with cracks of different severity. Dispersion characteristics of the propagating modes were evaluated through experiments and numerical simulations, where the obtained results were in agreement to each other. Time frequency analysis shows that certain modes have lower phase velocity in the area with cracks. In addition, the results demonstrate the capability of UGW to detect a crack that is invisible under visual inspection.

1 Introduction

Solar photovoltaics (PV) technology has emerged to be the popular option for power generation in the world continues the efforts towards net zero carbon emission target. The progress is endorsed not only by the advancement of technology and cost reduction of solar photovoltaic module (PVM), but also by the incentives through public policy in line with the Sustainable Development Goals. Rapid expansion in solar energy systems is indicated by the increase of PVM electricity generation capacity from 1.9 GW in 2010 up to over 133 GW in 2020 [1]. In the future, as solar power becomes a key element in global energy mix scenario, reliability of PVM systems turns into a crucial factor in order to maintain consistent supply into the electrical grid.

Predictive and preventive maintenance of solar PV systems includes structural health monitoring (SHM) of PVM. One of the important degradation modes in PVMs is the breakage or crack of glass or cell. In addition to compromising structural integrity, cracks allow moisture penetration that induces other damages and deterioration due to corrosion and discoloration [2].

Currently, several techniques are employed for PVMs inspection. Visual observation quickly identifies visible defects, yet lacking consistency and accuracy, especially in the case of microscale defects. Electroluminescence and Infrared thermography are the standard methods for fault detection in the cells and circuitry such as cell fracture, bad solder joint or inactive cells. Nevertheless, they are inefficient for detecting minor mechanical defects in PVM during operation [3, 4]. A conventional ultrasonic methods by pulse-echo or transmission scanning are powerful and mature techniques for high accuracy inspecting materials. The major drawback is that they are slow, hence impractical for in-situ inspection of large solar arrays.

A promising acoustic-based approach for PVMs evaluation is by using the ultrasonic guided waves (UGW) that propagate in the plate-like structure. In contrast to the conventional method, UGW can be transmitted over large distances, allowing long-range detection of defects, hence faster inspection process. Researchers have shown the potential of using Lamb waves analysis can be used to detect debonding and microcracks on polymer and composites layered structures, which are similar to PVM.

In this work, UGW will be employed for detecting cracks. The work is part of research in exploring the potential of UGW for a fast and reliable acoustic nondestructive inspection in PVM.

2 Methods

In this work, dispersion curves were first obtained through experiments and numerical simulation to identify the propagating Lamb waves modes. The obtained dispersion curves would be the basis for analyzing results from measurements on the defective part of a PVM.

The specimen was a thin-film-type PVM (SHARP NA-E315L) with cracks of different severity. Contact transducers with central frequency of 1 MHz were used as emitter and receiver, with water as couplant. To control the motion during measurements, transducers were mounted on a 5-axis scanning machine connected to a PC. In the experiments, a signal generator sent pulses of 500 kHz sinusoidal waves to the transmitter through an amplifier. The received signals were fed to a PC for visualization and data processing.

2.1 Numerical Simulations

Guided waves in a PVM model were simulated with DISPERSE to produce a plot of dispersion curves. The model was a 7-layer structure that represented a solar PVM, as shown in Figure 1.

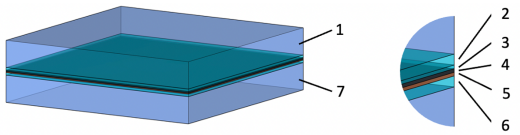

Figure 1 – Model of 7 layers structure representing a solar PVM used for numerical simulation

The solar cell assembly consists of silicon wafer with transparent conductive oxide (TCO) at the front and copper at the back side. The most common TCO for PVM is fluorine-doped tin oxide (FTO). That solar cell assembly is sandwiched between front and back panel glasses, bonded with ethylene vinyl acetate (EVA) encapsulant. Parameters set for each layer in Figure 1 are listed in Table 1.

Tableau 1 – Numerical simulation parameters

Layer	Mat'l	Thick. (mm)	Mechanical Properties		
			$\rho(g/cm^3)$	$E(GPa)$	ν
1,7	Glass	3.2	2.49	69.2	0.21
2,6	EVA	0.3	0.94	0.05	0.33
3	FTO	0.1	6.8	150	0.33
4	a-Si	0.1	2.23	130	0.33
5	Cu	0.1	7.8	110	0.33

2.2 Experiments

To obtain Lamb waves dispersion curves, an experiment was set up on an undamaged part of PVM specimen with an emitter fixed at a point while the receiver scanned along a line. The signals were recorded every 0.25 mm of the receiver's displacement, creating an array of time signals data of equally spaced points. Schematic of this experiment is illustrated in Figure 2. The acquired time signals at points of different distance between emitter and receiver were processed with 2D FFT method in MATLAB to generate a plot of frequency versus wavenumber.

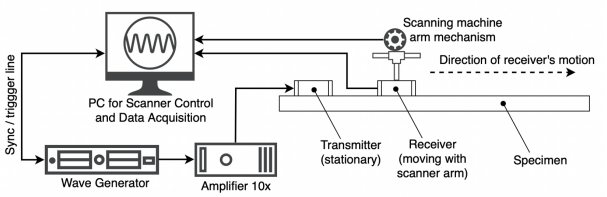

Figure 2 – Experimental setup to obtain Lamb waves dispersion curves

To investigate the interaction of ultrasound signals with damages within the structure, a section that contains cracks was chosen. In the selected section as shown in Figure 3, there exists a region with fine crack that is barely visible with eyes, which becomes the area of significant interest for a non-destructive evaluation. The distance between transducers was 60 mm and scanning length was 150 mm. At the position of 0 to 30 mm, there is no defect between transmitter and receiver. Between 30 mm and 75 mm there is visible crack that runs from the receiver scanning line to the middle of the investigated area. The other visible crack appears from 105 mm. However, those two visible cracks are suspected to be of one long crack, with the intermediate portion (75 mm to 105 mm) being a fine crack not detectable with visual inspection.

Experiment was conducted with the same equipment as the previously discussed Lamb waves dispersion curves measurements. The only difference was that in this experiment both transmitter and receiver were mounted on the scanning machine's moving arm, as depicted in Figure 4. Therefore, those transducers moved together while scanning, as opposed to the previous experiment where the transmitter was fixed and not attached to the scanner arm.

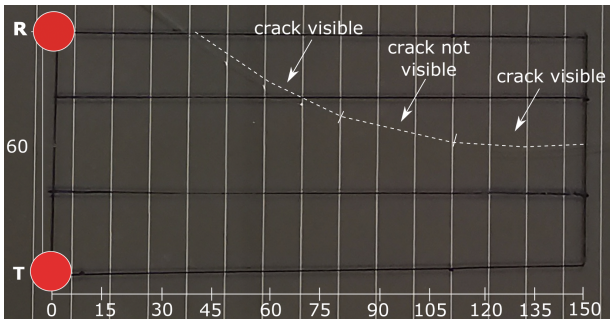

Figure 3 – Investigated area in the experiment of guided waves interaction with defects (Red T, R : transmitter and receiver starting position; scanning motion to the right; numbers are measurements in mm)

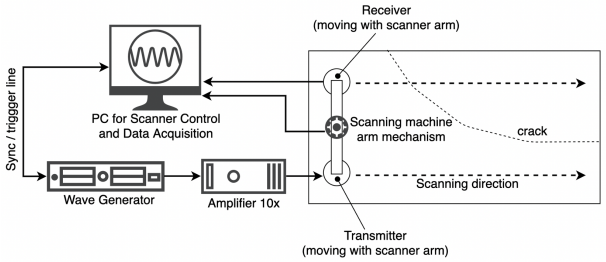

Figure 4 – Experimental setup to investigate interaction of guided waves with defects

3 Results

3.1 Dispersion characteristics of propagating waves

The signal in Figure 5 is a response on the receiver at a distance of 30 mm, 80 mm and 130 mm, respectively, from the transmitter. It demonstrates the change in waveform over the distance as it propagates in a dispersive medium.

To construct dispersion curves, 2D Fourier transform technique [7] was applied to time signals of the series of equally spaced distances which, acquired from the experiment. The intensity of the Fourier spectrum, represented by the color-scaled image in Figure 6, is distributed across the plot of frequency (f) versus wavenumber (k).

Numerical simulation yields dispersion curves that are overlaid in Figure 6 as continuous curved lines, with mode numbers automatically assigned by DISPERSE software. Referring to those lines, one can identify to which modes each high intensity color scale belongs to. In addition, the curves produced by numerical simulation closely match the actual propagating modes constructed from measurement data, which means that the model satisfactorily represents the real PVM specimen.

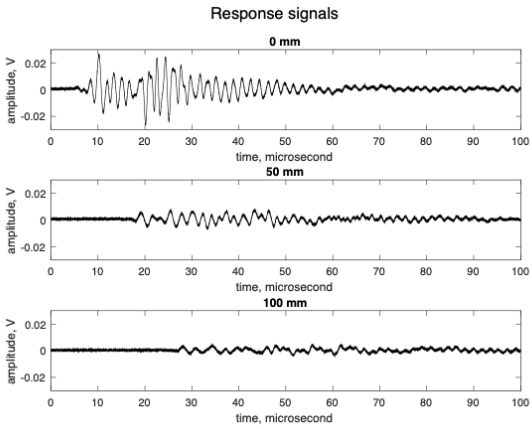

FIGURE 5 – Signal waveforms at 3 points of different distance from transmitter : 30 mm, 80 mm and 130 mm

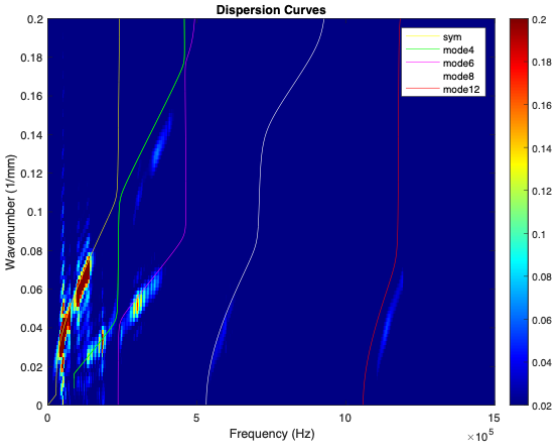

FIGURE 6 – Dispersion curves (color scaled image : experimental results ; lines : numerical results)

3.2 Interaction of guided waves with defect

Time-frequency analysis is employed to detect the change of velocity and/or mode conversion which can indicate the existence of material defects within the signal path [8]. Wavelet transform of a signal $f(t)$ is described in Equation 1, where a and t denote the scale and translation of wavelet, respectively. The mother wavelet chosen in this work is Morlet wavelet, aiming at higher time resolution [9]. In the equation, the mother wavelet function is denoted by ψ.

$$WT(a,t) = \frac{1}{\sqrt{2}} \int_{-\infty}^{\infty} f(t) * \psi\left(\frac{t-\tau}{a}\right) dt \qquad (1)$$

Continuous wavelet transform applied to the response signal acquired on the undamaged part of the observed section yields in a time-frequency diagram shown in Figure 7. Color scales indicate the magnitude of wavelet coefficients where highest intensity lies around 500 kHz, that is the excitation frequency of the transmitted signal in the experiment.

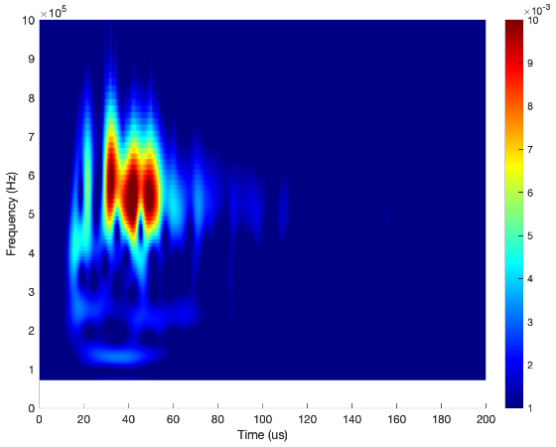

FIGURE 7 – Time-frequency diagram of the signal in the undamaged area)

Based on the hypothesis that there will be velocity changes or mode conversion upon encountering defects, the time-frequency distribution obtained from the undamaged area as depicted in Figure 7 will be different with those from defective areas. In other words, one will expect that the appearance of certain frequency can shift in time domain because of the change in velocity, if there is defect on its path. To allow observation on arrival time of a certain frequency at different points, the time series of a selected frequency in a time-frequency diagram is extracted and plotted for all position along scanning length. It creates a diagram that indicates the time of arrival of a particular frequency at every measurement position. Figure 8 (a) to (d) present the diagram for frequency of 140 kHz, 200 kHz, 300 kHz and 400 kHz. Those four frequencies are selected since they have possibilities of belonging to different modes according to the dispersion curves in Figure 6. Therefore, mode conversion can be observed if it occurs.

At all frequencies, there exists a high intensity region within the range of 15 us and 20 us. Knowing the distance between transducers in this experiment is 60 mm, the velocity is therefore between 3000 m/s to 4000 m/s which corresponds to Rayleigh wave/surface acoustic wave (SAW) velocity in glass [d,e]. The intensity of this wave is affected by the crack as one can see in all diagrams in Figure 8. The crack starts at the position of 20 mm, however the effect is not readily visible since the crack location is very close to the receiver, keeping in mind the size of the transducer represented by red circles in Figure 4. As the crack approaches the middle part of the observed section, changes in intensity can be noticed, first as a minor reduction at 70 mm at the onset of a fine crack region and then a significant drop in intensity at 110 mm where crack becomes visible again.

To analyze the velocity of modes, a frequency-phase velocity dispersion diagram in Figure 9, generated from numerical simulation, is used as the reference. The points in

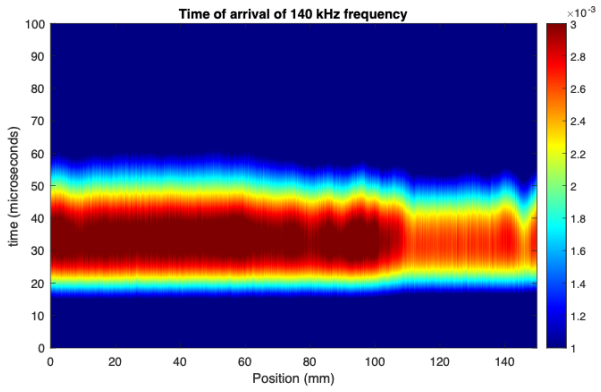

(a) 140 kHz

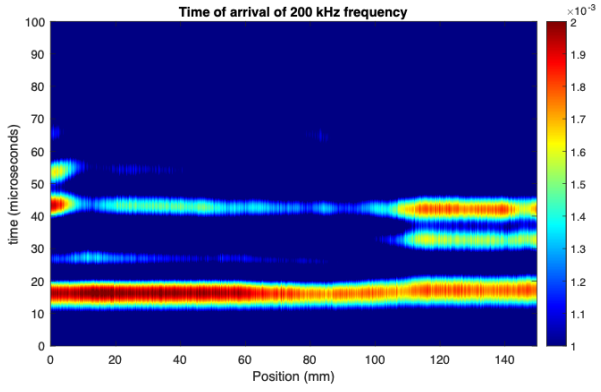

(b) 200 kHz

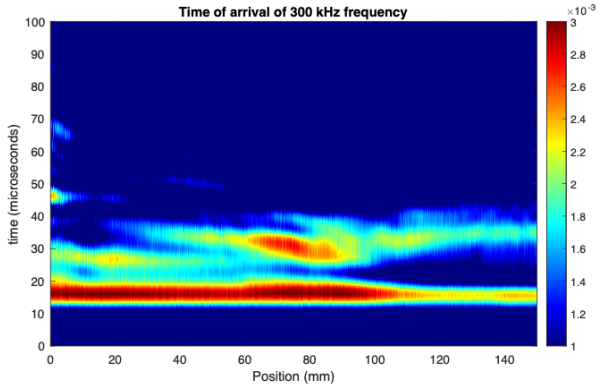

(c) 300 kHz

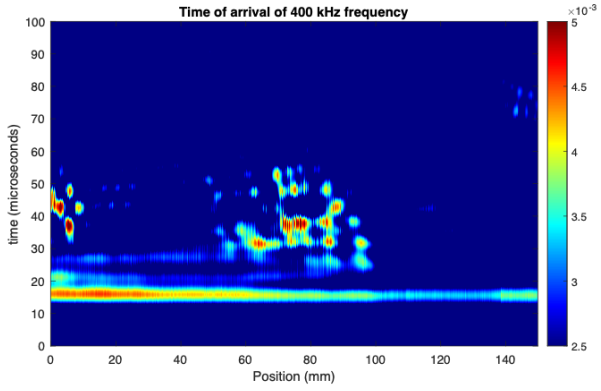

(d) 400 kHz

FIGURE 8 – Time of arrival of a particular frequency at different position. (Color scale indicates the magnitude of wavelet coefficient.)

the diagram mark the range of calculated average velocity of specific frequencies based on the time of occurrence of those frequencies in Figure 8.

From Figure 8 and 9, it can be inferred that the existence of crack in the path of guided waves causes a reduction of velocity, or slower time lag of arrival, of Lamb modes as seen in the case of 200 kHz and 300 kHz. At 400 kHz, the Lamb mode that appears in the pristine area is not detected in the response signal propagating through the crack, whereas SAW remains.

As mentioned earlier, the investigated area contains a section with fine crack not visible with visual inspection. This section (from 75 mm to 105 mm) shows high wavelet coefficient and lower phase velocity, as one can infer from Figure 8 (c) and (d). Therefore, UGW was able to detect that visually invisible crack.

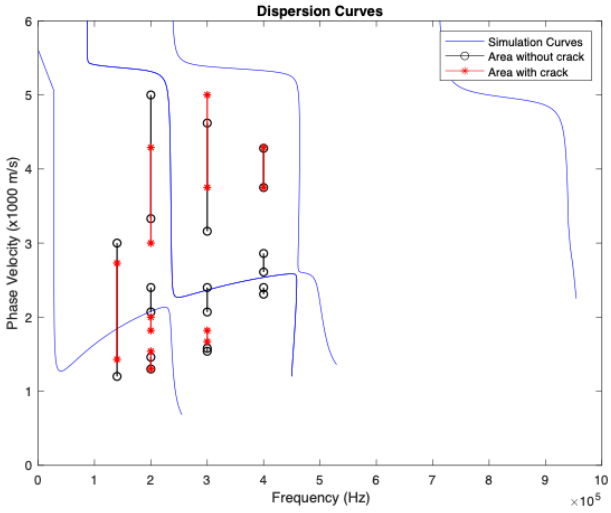

FIGURE 9 – Frequency – phase velocity dispersion curves, showing the range of velocities at particular frequencies calculated from the time of occurrence in Figure 8

4 Conclusion

In this work, detection of crack in solar PVM with guided waves is presented. Dispersion curves generated by numerical simulation software match closely with experimental results. It confirms that of the layered structure model implemented in simulations represents the actual structure. The generated dispersion curves also provide guidance to identify propagating modes for the purpose of studying Lamb modes characteristics. Time frequency analysis on the response signals reveals that phase velocities of certain modes decrease in the area with crack. In addition, a fine crack that is unseen with visual inspection is detected through Lamb waves analysis. Therefore, UGW technique is a promising means of a non-destructive inspection of solar PVM.

Références

[1] A. Jäger-Waldau, I. Kougias, N. Taylor, C. Thiel, How photovoltaics can contribute to GHG emission reductions of 55% in the EU by 2030, *Renewable and Sustainable Energy Reviews* **126**, (2020).

[2] M.A. Quintana, D.L. King, T.J. McMahon, C.R. Osterwald, Commonly observed degradation in field-aged photovoltaic module, In *Proceedings of the Conference Record of the Twenty-Ninth IEEE Photovoltaic Specialists Conference*, 1436-1439 (2020).

[3] J. Kim, M. Rabelo, S.P. Padi, H. Yousuf, E.-C. Cho, J. Yi, A review of the degradation of photovoltaic modules for life expectancy, *Energies* **14**, (2021).

[4] G. Balasubramani, V. Thangavelu, M. Chinnusamy, U. Subramaniam, S. Padmanaban, L. Mihet-Popa, Infrared thermography based defects testing of solar photovoltaic panel with fuzzy rule-based evaluation, *Energies* **13**, (2020).

[5] M. Liu, S. Chen, Z.Z. Wong, K. Yao, F. Cui, In situ disbond detection in adhesive bonded multi-layer metallic joint using time-of-flight variation of guided wave, *Ultrasonics* **102**, (2020).

[6] S. Yaacoubi, L. Chehami, M. Aouini, N. Declercq, Ultrasonic guided waves for reinforced plastics safety, *Reinforced Plastics* **61**(2), 87-91 (2017).

[7] D. Alleyne and P. Cawley, A two-dimensional Fourier transform method for the measurement of propagating multimode signals, *The Journal of the Acoustical Society of America* **89**, 1159 (1991).

[8] Demčenko, E. Žukauskas, R. Kažys, A. Voleišis, Interaction of the A0 Lamb wave mode with a de-lamination type defect in GLARE3-3/2 composite material, *Acta Acustica united with Acustica* **92**, 540-548 (2006).

[9] G. Zhao, B. Wang, T. Wang, W. Hao, Y. Luo, Detection oand monitoring of delamination in composite laminates using ultrasonic guided waves, *Composite Structures* **225**, (2019).

[10] S. Dondeti, H.V. Tippur, A comparative study of dynamic fracture of soda-lime glass using photoelasticity, digital image correlation and digital gradient sensing techniques, *Experimental Mechanics* **60**, 217-223 (2020).

[11] Y. Terakawa, J. Kondoh, Numerical and experimental study of acoustic wave propagation in glass plate/water/128YX-LiNbO3 structure, *Japanese Journal of Applied Physics* **59**, (2020).